Geomechanics and Engineering, *Vol. 38, No. 6 (2024) 611-620*
https://doi.org/10.12989/gae.2024.38.6.611

A study on slope design at tunnel portal considering impact of blasting

Ji-Ung Lee[1a], Jee-Hee Jung[2b], Kang-Hyun Lee*[2], SangRae Lee[2c] and Nag-Young Kim[2d]

[1]*Department of Architectural Engineering, Chung-Ang University, 84, Heukseok-ro, Dongjak-gu, Seoul 06974, Republic of Korea*
[2]*Safety Innovation& Disaster Prevention Research Division, Korea Expressway Corporation Research Institute, 24, Dongbusunhwan-daero 17-gil, Hwaseongsi, Gyeonggi-do 18489, Republic of Korea*

(*Received November 23, 2023, Revised January 23, 2024, Accepted February 2, 2024*)

Abstract. The slope stabilization method is constructed on bedrock, but performance degradation occurs during an impact (earthquake, blasting, etc.) after construction, which may affect service life and factor of safety. In particular, the top-down method implies the possibility of damage caused by blasting vibration due to the construction procedure. However, the current blasting design only reflects damage to nearby facilities, so there is a limit in its ability to assess the damage of reinforcement methods caused by blasting vibration within the scope of influence. In this study, we aim to evaluate problems and damage levels caused by close blasting effects on rock-integrated structures, such as panel-type retaining walls, anchor-combined structures, and small nails, which are mainly constructed using the top-down method. We will also analyze factors affecting long-term performance according to changes in conditions after construction, such as tunnel excavation, to establish optimal design measures.

Keywords: blasting effects; cutting slope; tunnel blasting; tunnel portal

1. Introduction

Recently constructed expressways in mountainous areas often experience environmental damage due to slope cutting. To mitigate this issue, there is an increasing trend of implementing reinforcement methods on the upper soil layer to minimize cutting heights. Additionally, tunnel construction is becoming more prevalent for new expressways to reduce geological constraints and environmental damage.

When designing tunnels, the focus is on eco-friendly practices that aim to minimize damage to the natural surroundings of the tunnel portal. Consequently, the slope reinforcement method is being utilized more extensively than in the past. However, when these reinforcement methods are applied to the slope, there might be interference with the tunnel reinforcement method. Currently, there are no standard guidelines for the interference range (appropriate separation distances). This lack of a standard raises concerns about potential interference during construction, which could compromise the performance and stability of the overall structure. Depending on the level of interference, there is concern that the performance of the reinforcement method during construction could deteriorate and affect the stability of the structure (Kim and Lee 2021).

Many studies have been conducted on the stability of slopes and tunnels (Deng *et al.* 2019, Tran *et al.* 2019, Jin *et al.* 2022, Hu *et al.* 2023, Kim *et al.* 2023). However, specific studies on tunnel portal slopes affected by tunnel blasting has not been conducted, thus failing to provide quantitative values or criteria for slope design during tunnel excavation.

Therefore, this study aims to establish an optimal design plan for the tunnel portal by analyzing the characteristics, considering the effect of proximity blasting on the reinforcement method of cutting slop and the interference between the reinforcement of tunnel and slope.

2. Numerical analysis

2.1 Analysis of influencing factors

2.1.1 Summary

To assess the impact of blasting vibrations on the retaining wall of the slop, a 3-dimensional analysis of the tunnel portal was conducted using the MIDAS GTS NX program developed by MIDAS Information Technology Co. When modelling infinite materials like the ground, in a static analysis, it suffices to set boundaries far enough away. However, in dynamic analysis, using typical boundaries can cause significant errors due to wave reflections. Methods to address this include approximate methods like artificial boundaries, transmitting boundaries/hyper elements, infinite elements, and boundary elements. In this analysis, the viscous boundary proposed by Lysmer and Wass in 1972 (also known as the viscous or quiet boundary) was applied (Choi *et al*. 2006).

*Corresponding author, Ph.D., Principal Researcher
E-mail: tunnelslope@ex.co.kr
[a]Ph.D. Candidate
[b]Ph.D.
[c]Ph.D. Candidate
[d]Ph.D.

ISSN: 2005-307X (Print), 2092-6219 (Online)

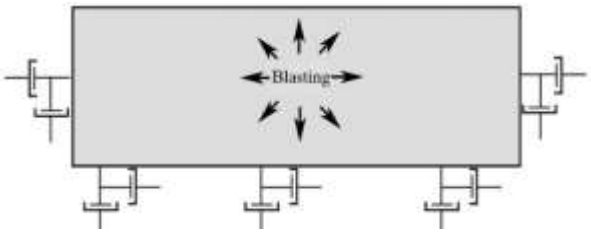

Fig. 1 Viscous boundary

Eigenvalue analysis is used to analyse the inherent dynamic characteristics of structures, also known as Free vibration analysis. In this analysis, the eigenvalues (or natural frequencies) of the first and second modes obtained through eigenvalue analysis are determined to obtain damping matrices used in time history analysis.

In this analysis, a time history analysis is performed to interpret the dynamic behavior of the structure under dynamic loading, specifically the blast loads. To interpret the dynamic response of the structure under dynamic loading, the Newmark method with good convergence is used to perform direct integration.

1.2 Estimation of blasting loads

The blast pressure uses estimated pressure values derived from theoretical calculation equations and empirical equations. The Eq. (1) presented by the National Highway Institute (US) in 1991 was applied.

$$P_d = \frac{4.18 \times 10^{-7}(\rho V^2)}{1 + 0.8\rho}, \qquad P_B = P_d \times (\frac{d_c}{d_h})^3 \qquad (1)$$

Here, P_d: Detonation pressure (kbar)
P_B: Decoupled detonation pressure (kbar)
ρ: Explosive density (g/cm3)
V: Blast velocity (ft/sec)
d_c: Charge diameter (mm)
d_h: Borehole diameter (mm)

Subsequently, to account for the reduction in blast vibration, the equation considering the decoupling effect was utilized to calculate the dynamic pressure varying with time acting on the actual walls. This was computed using the Eq. (2) proposed by Starfield and Pugliese (Starfield and Pugliese 1968).

$$P_D(t) = 4P_B(\exp\left(\frac{-Bt}{\sqrt{2}}\right) - \exp(-\sqrt{2}Bt)) \qquad (2)$$

Here, B: Load constant (16,338)
t: Duration of the load due to the blast

The purpose is to observe the response at intervals from a section away from the blast and modelling the blast hole as an element is difficult. Therefore, assuming the explosive charges are concentrated in one place and act distributed over the predicted blast surface with the same pressure lag, an equivalent P_B was calculated and used for analysis (Min *et al*. 2005, Lee *et al*. 2011).

2.1.3 Analysis results

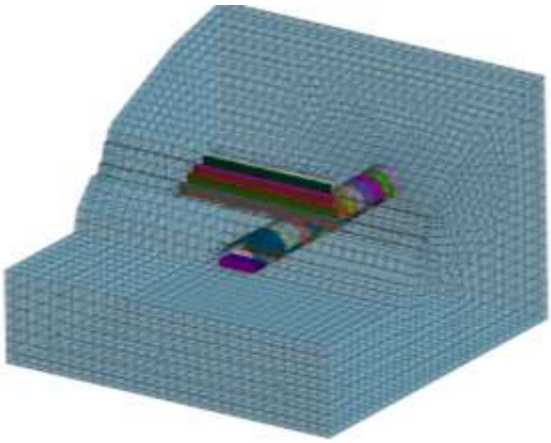

Fig. 2 3D modelling of the tunnel portal

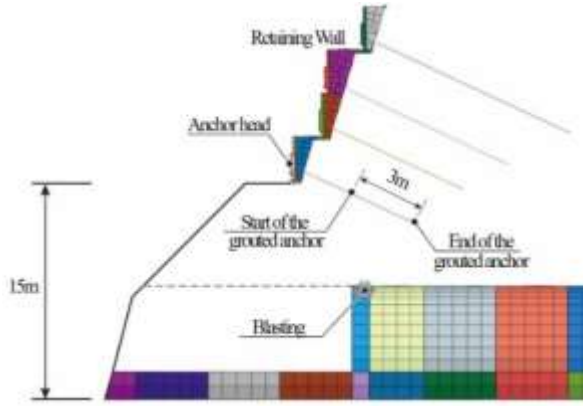

Fig. 3 Measurement location

The 3D modelling aimed to consider the geological characteristics of the tunnel portal, the influence of the tunnel cross section, and the three-dimensional behavior of blast vibrations. The modelling is illustrated in Fig. 2. To understand the influencing factors for each CASE, the stratum was assumed to consist of a single layer. The retaining wall was positioned 15 meters above the tunnel floor, and the simulation involved four layers of retaining walls. Anchors of varying lengths (9.5 m, 11 m, 14 m, and 16 m) were installed in sequence from the first layer, all with a 25° downward slope. The anchor bond length was assumed to be 3 meters.

The analysis results of the blasting effects were reviewed (see Fig. 3), focusing on the dynamic modulus of elasticity (CASE-1), the damping ratio (CASE-2) and the charge weight per delay (CASE-3).

Blasting vibrations involve vibration with amplitude and frequency, the magnitude of which can be represented by the particle displacement, particle velocity, and particle acceleration of the transmitting medium (M.L.I.T. 2020).

The assessment of blast vibration considered the displacement between the cutting slope retaining wall installed on the tunnel back side and the tunnel blasting point, the dynamic modulus of elasticity (E_d), and the damping ratio (ε). The applied cases for the analysis are summarized in Table 1.

Table 1 Analysis cases

			Dynamic modulus of elasticity (E_d, MPa)	Dynamic poissons ratio(ν_d)	Damping ratio (ξ, %)	Charge weight per delay (kg)
Effects according to the dynamic modulus of elasticity	Case1	Case1-1	2,500	0.24	8	0.25
		Case1-2	10,000	0.24	8	0.25
		Case1-3	15,000	0.24	8	0.25
Effects according to the damping ratio	Case2	Case2-1	10,000	0.24	10	0.25
		Case2-2	10,000	0.24	8	0.25
		Case2-3	10,000	0.24	3.5	0.25
Effects according to the charge weight per delay	Case3	Case3-1	10,000	0.24	8	0.25
		Case3-2	10,000	0.24	8	1.00
		Case3-3	10,000	0.24	8	1.50
		Case3-4	10,000	0.24	8	1.75

Table 2 Analysis results on the effect of the dynamic modulus of elasticity

Case	Dynamic modulus of elasticity (MPa)	Maximum vibration velocity (cm/sec, Kine)			Maximum Displacement (mm)		
		End of the grouted anchor body	Start of the grouted anchor body	Anchor head (retaining wall)	End of the grouted anchor body	Start of the grouted anchor body	Anchor head (retaining wall)
1-1	2500	0.003308	0.002693	0.001089	0.000113	0.000090	0.000084
1-2	10,000	0.003238	0.002424	0.001153	0.000057	0.000045	0.000043
1-3	15,000	0.003228	0.002351	0.001178	0.000046	0.000037	0.000036

Table 3 Analysis results on the effect of the damping ratio

Case	Damping ratio (%)	Maximum vibration velocity (cm/sec, Kine)			Maximum Displacement (mm)		
		End of the grouted anchor body	Start of the grouted anchor body	Anchor head (retaining wall)	End of the grouted anchor body	Start of the grouted anchor body	Anchor head (retaining wall)
2-1	10.0	0.003130	0.002315	0.001014	0.000052	0.000040	0.000039
2-2	8.0	0.003238	0.002424	0.001153	0.000057	0.000045	0.000043
2-3	3.5	0.004169	0.004575	0.002000	0.000074	0.000069	0.000060

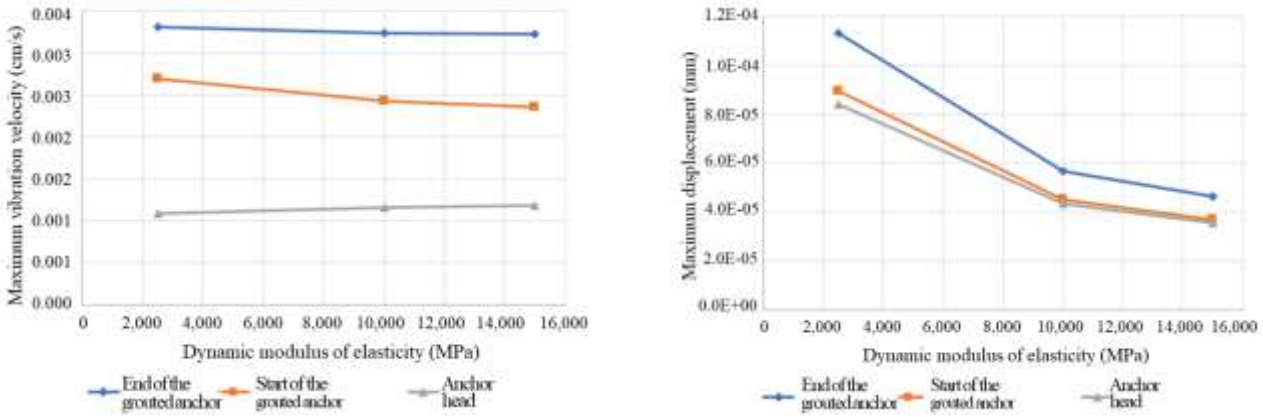

(a) Maximum vibration velocity (b) Maximum displacement

Fig. 4 Trends in maximum vibration velocity and maximum displacement for CASE 1

When analyzing the impact of the dynamic modulus of elasticity, it was noticed that the difference between the vibration velocity and the maximum displacement result was relatively small. As the dynamic modulus of elasticity increased (closer to the blast rock), both the displacement and vibration velocity tended to decrease. The vibration

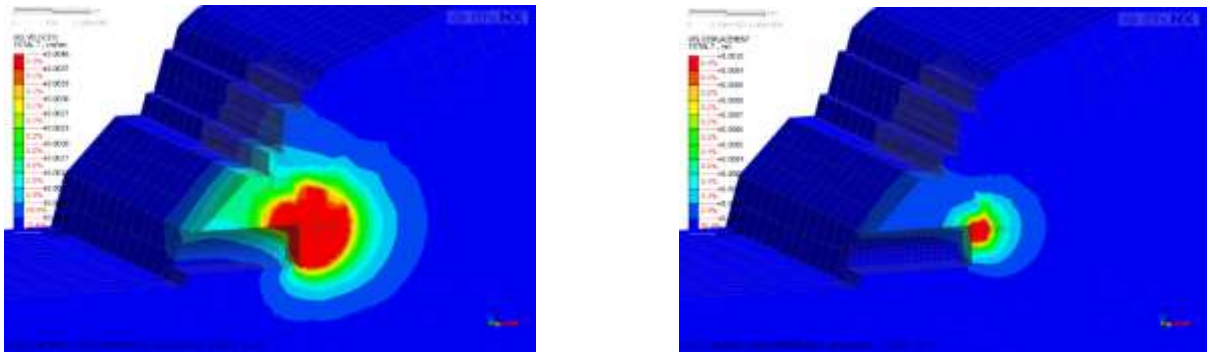

(a) Maximum vibration velocity (b) Maximum displacement

Fig. 5 Results in maximum vibration velocity and maximum displacement for CASE 1-1

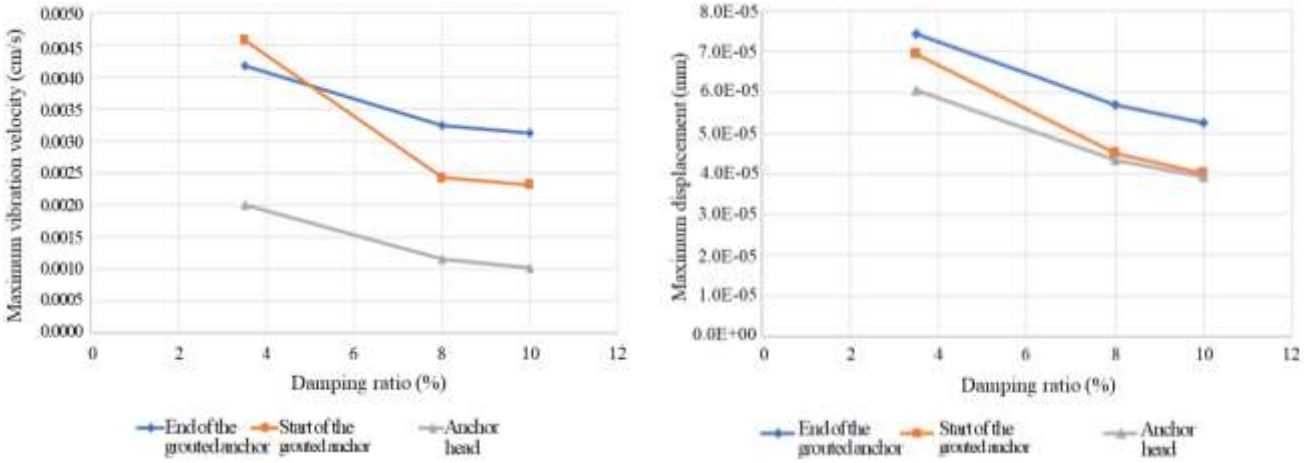

(a) Maximum vibration velocity (b) Maximum displacement

Fig. 6 Trends in maximum vibration velocity and maximum displacement for CASE 2

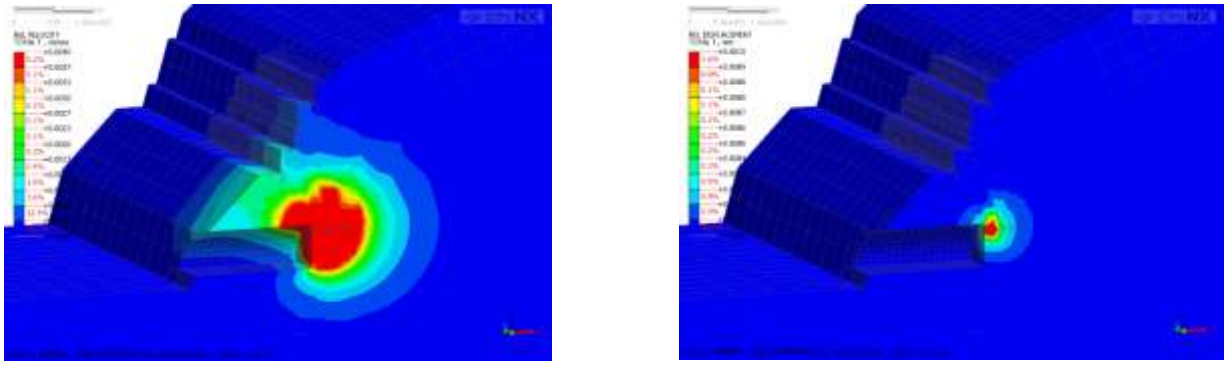

(a) Maximum vibration velocity (b) Maximum displacement

Fig. 7 Results in maximum vibration velocity and maximum displacement for CASE 2-1

velocity at the end of the grouted anchor body was approximately 3 times higher than at the retaining wall. The displacement at the end of the grouted anchor body was approximately 1.4 times greater than at the retaining wall.

Moreover, increasing the dynamic modulus of elasticity resulted in shorter arrival times for vibrations, indicating faster propagation (see Table 2, Figs. 4 and 5).

Based on the analysis of the damping ratio's effect, it was observed that the vibration velocity decreased as the damping ratio increased. Additionally, the displacement also decreased with an increase in the damping ratio.

Furthermore, the vibration velocity difference between the end of the grouted anchor body and the retaining wall was approximately 1.5 times greater at the end of the grouted anchor body. Likewise, the displacement at the end of the grouted anchor body was 1.3 times greater compared to that of the retaining wall (see Table 3, Figs. 6 and. 7).

As a result of analyzing the effect of the charge weight per delay at each major point of the retaining wall, it was observed that both the vibration velocity and displacement increased linearly with an increase in the charge weight per delay (see Table 4, Figs. 8 and 9).

Table 4 Analysis results on the effect of the charge weight per delay

Case	Charge weight per delay (kg)	Maximum vibration velocity (cm/sec, Kine)			Maximum Displacement (mm)		
		End of the grouted anchor body	Start of the grouted anchor body	Anchor head (retaining wall)	End of the grouted anchor body	Start of the grouted anchor body	Anchor head (retaining wall)
3-1	0.25	0.003238	0.002424	0.001153	0.000057	0.000045	0.000043
3-2	1.00	0.012723	0.009536	0.004532	0.000223	0.000177	0.000170
3-3	1.50	0.019085	0.014304	0.006798	0.000335	0.000265	0.000255
3-4	1.75	0.022266	0.016688	0.007931	0.000391	0.000309	0.000298

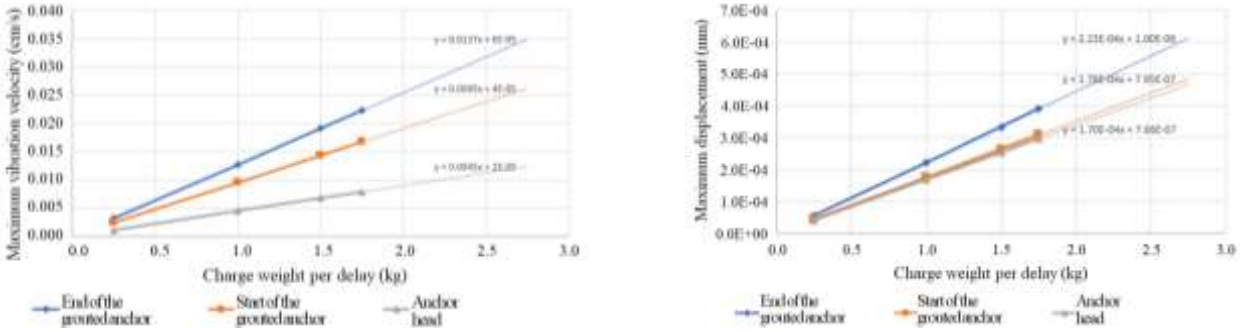

(a) Maximum vibration velocity (b) Maximum displacement

Fig. 8 Trends in maximum vibration velocity and maximum displacement for CASE 3

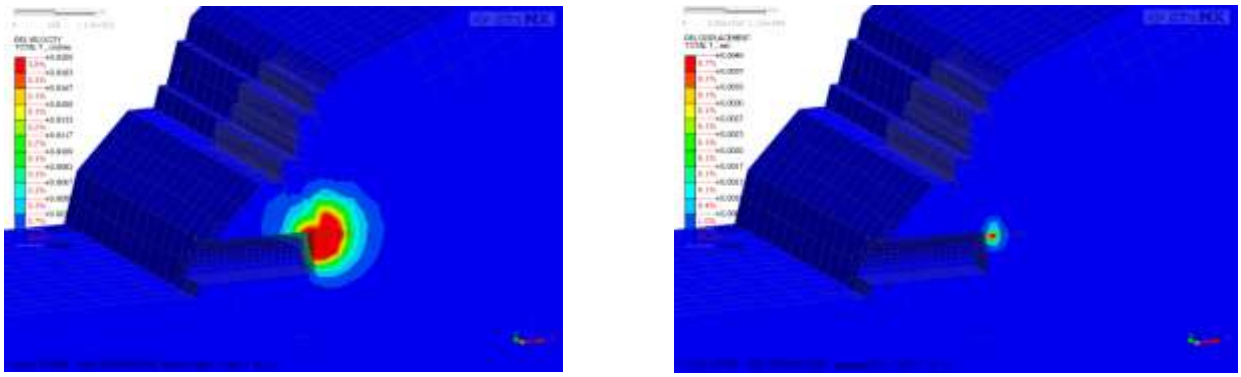

(a) Maximum vibration velocity (b) Maximum displacement

Fig. 9 Results in maximum vibration velocity and maximum displacement for CASE 3-1

Table 5 Charge weight per delay

	Low vibration	Precision vibration	Small scale	Medium scale	General blasting I	General blasting II
Change weight per delay(kg)	0.125	0.500	1.250	3.000	5.000	7.500

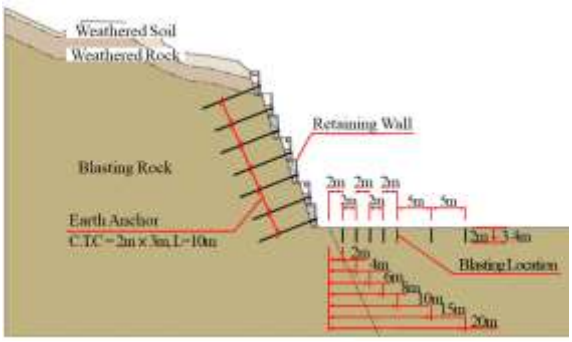

Fig. 10 Analysis conditions of blasting vibration

2.2 Damage characteristics of reinforced structures

In the analysis of the damage characteristics of reinforced structures through numerical analysis, the study considered general design conditions to investigate the impact of blasting vibration on the retaining wall (K.E.C.R.I. 2017). Numerical analysis was conducted with variations in the distance from the retaining wall and the charge weight per delay. The analysis section was applied as illustrated in Fig. 10, and 7 separation distances ranging from 2 to 20 meters were utilized for the distance from the retaining wall. Additionally, the charge weight per delay was analyzed under 6 conditions, as shown in Table 5, resulting in a total of 42 cases for numerical analysis.

For the analysis of the vibration impact on the retaining wall structure and changes in anchor axial force, the

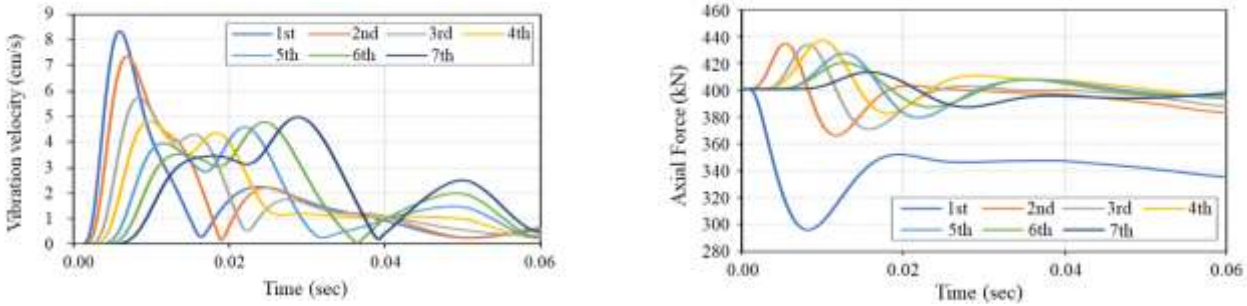

(a) Vibration velocity trends at the grouted anchor body (b) Variation trends of anchor jacking force

Fig. 11 Evaluation results of ground anchors

Table 6 Blasting vibration velocity results through numerical analysis (Charge Weight: 0.125 kg)

Separation distance	Generated vibration velocity(cm/sec)									
	Anchor head					Grouted anchor body				
	Scale distance	Numerical analysis	M.L.I.T.*	On-site estimated equations		Scale distance	Numerical analysis	M.L.I.T.*	On-site estimated equations	
				Square	Cube				Square	Cube
2 m	15.4	1.154	4.376	3.219	1.986	37.3	0.561	1.062	0.795	0.509
4 m	19.8	0.960	2.932	2.167	1.351	43.0	0.489	0.848	0.636	0.409
6 m	24.7	0.786	2.059	1.529	0.961	48.6	0.433	0.695	0.523	0.338
8 m	30.0	0.648	1.509	1.125	0.713	54.3	0.387	0.583	0.440	0.286
10 m	35.1	0.536	1.174	0.878	0.560	60.0	0.347	0.498	0.376	0.245
15 m	48.9	0.353	0.689	0.519	0.335	74.1	0.273	0.354	0.269	0.177
20 m	62.8	0.249	0.462	0.350	0.228	88.2	0.213	0.268	0.204	0.135

*Ministry of Land, Infrastructure and Transport

measurement points were set at the anchor head and the grouted anchor body at the bottom of the retaining wall.

This aimed to understand the trends based on changes in separation distance and Charge weight per delay.

The analysis sections of the retaining wall were divided into 7 segments (from 1st to 7th segments), reviewing the impact of blasting on each segment and summarizing the results based on the segment with the most significant impact.

A representative summary was conducted for a charge weight per delay of 3.0 kg and a separation distance of 2m from the slope. As shown in Fig. 11, the closest segment (1st segment) to the blasting point exhibited the highest vibration velocity. As moved from the 2nd to the 7th segment, a decreasing trend in vibration velocity was observed. Additionally, the most substantial decrease in jacking force occurred in the 1st segment, with diminishing jacking force reduction observed from the 2nd to the 7th segment.

2.2.1 Vibration velocity variation

The analysis focused on the trend of blasting vibration velocities (cm/sec) at the anchor head and the grouted anchor body at the bottom of the retaining wall. The blasting vibration velocities based on the scale distance are detailed in Tables 6 and 7.

The generated vibration velocities of the anchor head and the grouted anchor body, installed on the slope due to the tunnel blasting, were compared using numerical analysis methods, as well as with the methods proposed by the MLIT (Ministry of Land, Infrastructure and Transport), and an on-site estimation equation (K.E.C. 2019, M.L.I.T. 2020). The comparison showed that as the distance from the slope increased, the vibration velocities calculated through numerical analysis tended to be greater than those estimated by the MLIT equation and the on-site estimation equation.

Based on the analysis of blasting vibrations, the following trend of blasting vibration velocity at the end of the grouted anchor body and the anchor head is shown in Table 8. The vibration velocity generated at the end of the grouted anchor body, when measured at the same distance from the slope, was found to be 47.5% to 87.9% of that compared to the anchor head. This difference in vibration velocity is attributed to the variation in distance from the blasting point.

The review of blasting vibration impact based on the estimation equation provided by the MLIT resulted in the vibration velocity occurrence trends at the retaining wall's anchor head and grouted anchor body as shown in Table 9.

For the grouted anchor body, applying an explosive charge of 7.5 kg (general blasting), the permissible vibration velocity exceeding 12.7 cm/sec was observed within a scaled distance of 5.6 m or less. Concerning the anchor head, with an explosive charge of 1.2 5 kg (small-scale blasting), the permissible vibration velocity exceeding 12.7 cm/sec was observed within a scaled distance of 4.9 m or less. When applying an explosive charge of 3.0 kg (lower limit of medium-scale blasting), the permissible vibration

Table 7 Blasting vibration velocity results through numerical analysis (Charge Weight: 7.500 kg)

Separation distance	Generated vibration velocity(cm/sec)									
	Anchor head					Grouted anchor body				
	Scale distance	Numerical analysis	M.L.I.T.*	On-site estimated equations		Scale distance	Numerical analysis	M.L.I.T.*	On-site estimated equations	
				Square	Cube				Square	Cube
2 m	2.0	57.222	66.503	47.278	27.251	4.8	30.438	16.149	11.685	6.978
4 m	2.6	47.624	44.557	31.835	18.535	5.6	27.137	12.886	9.351	5.616
6 m	3.2	40.112	31.293	22.457	13.191	6.3	24.145	10.573	7.691	4.642
8 m	3.9	34.118	22.939	16.526	9.783	7.0	21.666	8.867	6.464	3.919
10 m	4.5	29.321	17.848	12.899	7.684	7.7	19.577	7.567	5.527	3.364
15 m	6.3	20.681	10.476	7.621	4.601	9.6	15.725	5.392	3.956	2.428
20m	8.1	14.493	7.029	5.139	3.134	11.4	12.594	4.077	3.002	1.855

*Ministry of Land, Infrastructure and Transport

Table 8 The trend of blasting vibration velocity (Numerical analysis)

	Allowable blasting vibration velocity range exceeding 12.7 cm/sec
End of the grouted anchor body	■ 7.5 kg of Charge weight per delay (general blasting): exceeded within 9.6 m of scale distance ■ 5.0 kg of Charge weight per delay (maximum for medium scale blasting): exceeded within 9.5 m of scale distance ■ 3.0 kg of Charge weight per delay (lower limit for medium scale blasting): within the allowable value for all sections
Anchor head (retaining wall)	■ 7.5 kg of Charge weight per delay (general blasting): exceeded within 8.1 m of scale distance ■ 5.0 kg of Charge weight per delay (maximum for medium scale blasting): exceeded within 7.7 m of scale distance ■ 3.0 kg of Charge weight per delay (lower limit for medium scale blasting): exceeded within 4.0 m of scale distance ■ 1.25 kg of Charge weight per delay (small scale blasting): within the allowable value for all sections

Table 9 The trend of blasting vibration velocity (Ministry of Land, Infrastructure and Transport)

	Allowable blasting vibration velocity range exceeding 12.7 cm/sec
End of the grouted anchor body	■ 7. 5 kg of Charge weight per delay (general blasting): exceeded within 5.6 m of scale distance ■ 5.0 kg of Charge weight per delay (maximum for medium scale blasting): within the allowable value for all sections
Anchor head (retaining wall)	■ 7.5 kg of Charge weight per delay (general blasting): exceeded within 4.5 m of scale distance ■ 5.0 kg of Charge weight per delay (maximum for medium scale blasting): exceeded within 5.5 m of scale distance ■ 3.0 kg of Charge weight per delay (lower limit for medium scale blasting): exceeded within 5.0 m of scale distance ■ 1.25 kg of Charge weight per delay (small scale blasting): exceeded within 4.9 m of scale distance ■ 0.50 kg of Charge weight per delay (precision vibration): within the allowable value for all sections

velocity exceeding 12.7 cm/sec was observed within a scaled distance of 5.0 m or less. With an explosive charge of 5.0 kg (upper limit of medium-scale blasting), the permissible vibration velocity exceeding 12.7 cm/sec was observed within a scaled distance of 5.5 m or less. Finally, using an explosive charge of 7.5 kg (typical blasting), the permissible vibration velocity exceeding 12.7 cm/sec was observed within a scaled distance of 4.5 m or less.

The review of blasting vibration impact based on on-site estimation revealed the vibration trends at the grouted anchor body and anchor head of the retaining wall, as presented in Table 10.

For the grouted anchor body, all review conditions indicated vibration velocities within the permissible limit of 12.7 cm/sec. Regarding the anchor head, when applying an explosive charge of 3.0 kg (lower limit of medium-scale blasting), results showed exceeding the allowable vibration velocity of 12.7 cm/sec from within a scaled distance of 4 m. When applying an explosive charge of 5.0 kg (maximum for medium-scale blasting), the allowable vibration velocity was exceeded from within a scaled distance of 3.9 m. Additionally, when applying an explosive charge of 7.5 kg (general blasting), the allowable vibration velocity was exceeded from within a scaled distance of 4.5 m.

Comparative review between the MLIT's method and numerical analysis revealed that for an explosive charge of 1.25kg (small-scale blasting), both numerical analysis and the MLIT's method showed similar results. As the charge weight per delay increased, numerical analysis demonstrated higher blasting vibration velocities compared to the MLIT's method. Conversely, as the charge weight per delay decreased, the MLIT's method indicated higher vibration velocities compared to numerical analysis.

2.2.2 Evaluation of numerical analysis results

An analysis was conducted on data from 1,444 test

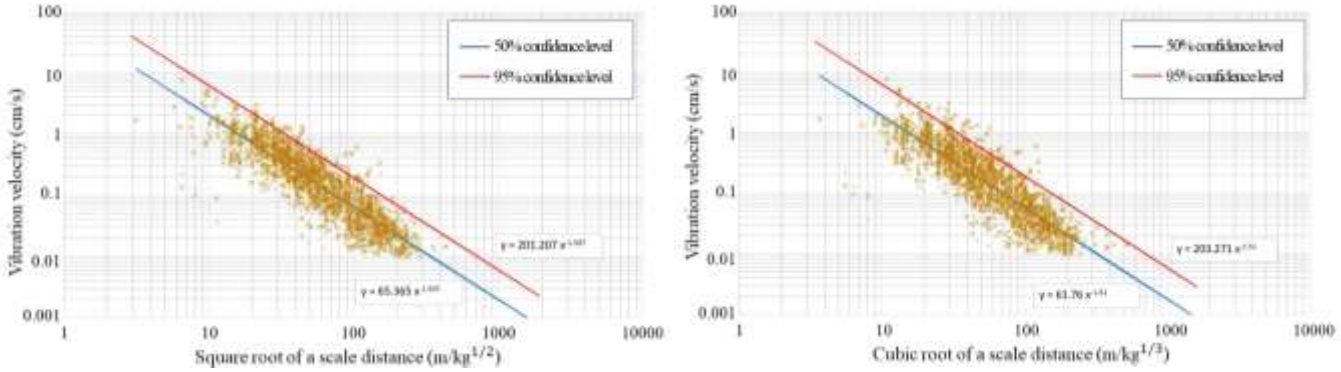

(a) Square root (b) Cubic root

Fig. 12 Blasting vibration velocities based on scale distance (Case analysis of the most recent 50 sites)

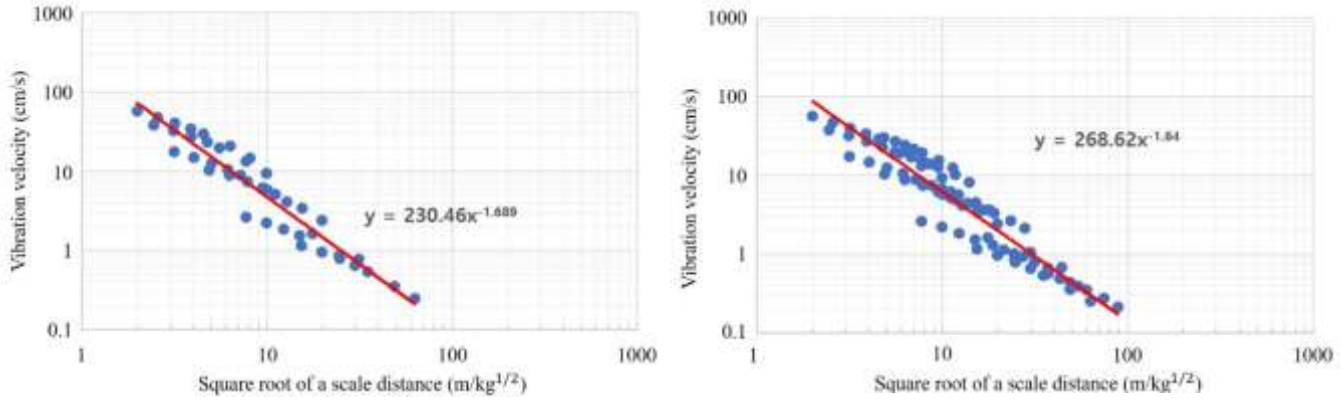

(a) Anchor head (b) Anchor head and grouted anchor body

Fig. 13 Blasting vibration velocities based on scale distance (Numerical analysis)

Table 10 The trend of blasting vibration velocity (On-site)

	Allowable blasting vibration velocity range exceeding 12.7 cm/sec
End of the grouted anchor body	■ All case : within the allowable value for all sections
Anchor head (retaining wall)	■ 7.5 kg of Charge weight per delay (general blasting): exceeded within 4.5 m of scale distance ■ 5.0 kg of Charge weight per delay (maximum for medium scale blasting): exceeded within 3.9 m of scale distance ■ 3.0 kg of Charge weight per delay (lower limit for medium scale blasting): exceeded within 4.0 m of scale distance ■ 1.25 kg of Charge weight per delay (small scale blasting): within the allowable value for all sections

blasting instances carried out in civil and building construction sites over the past five years (2017-2021). The blasting vibration velocities based on the scale distance are showed in Figs. 8 and 9 (DL E&C 1998, Kim and Lee 2021).

Results from test blasting conducted at 50 sites revealed estimation equations for blasting vibration velocities based on the scale distance with a 95% confidence level, and these were compared with the estimation equations derived from numerical analysis results, as shown in Table 11.

Table 11 Comparison of blasting vibration trends

Test blasting data from 50 sites		Numerical analysis results	
Square Root	$y = 201.207x^{-1.507}$	Anchor head	$y = 230.46x^{-1.689}$
Cubic root	$y = 203.271x^{-1.51}$	Anchor head and grouted anchor body	$y = 268.62x^{-1.64}$

*y: Blasting vibration velocity (cm/s), x: Scale distance (m/kg)

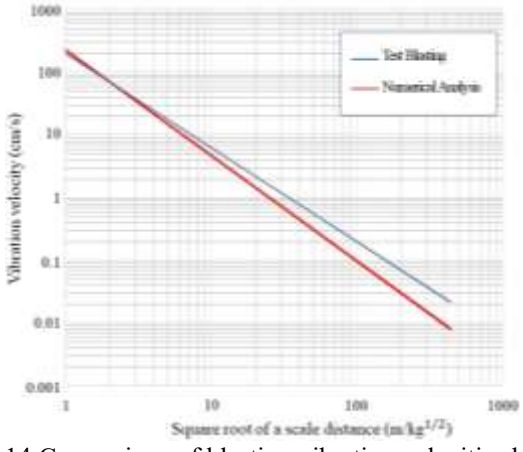

Fig. 14 Comparison of blasting vibration velocities based on the scale distance

Table 12 Influence range on slopes based on charge weight per delay (Unit: cm/sec)

Separation distance	Test blasting 50 cases estimation equation						Separation distance	Numerical analysis estimation equation					
	Non-vibration	Precision Vibration	Small-scale	Medium-scale	General	Large-scale		Non-vibration	Precision Vibration	Small-scale	Medium-scale	General	Large-scale
	0.125 kg	0.50 kg	1.6 kg	5.00 g	15.0 kg	20.0 kg		0.125 kg	0.50 kg	1.6 kg	5.00 g	15.0 kg	20.0 kg
1.0 m	41.99	119.35	286.71	676.58	1,548.2	1,923.0	1.0 m	39.80	128.34	342.75	897.17	2,268.8	2,892.8
2.3 m	11.97	34.02	81.72	192.84	441.27	548.08	2.0 m	12.35	39.80	106.30	278.25	703.66	897.17
4.5 m	4.35	12.37	29.72	70.13	160.49	199.33	4.0 m	3.83	12.35	32.97	86.30	218.24	278.25
8.0 m	1.83	5.20	12.49	29.47	67.43	83.76	7.1 m	1.45	4.68	12.51	32.74	82.80	105.57
14.0 m	0.79	2.24	5.37	12.68	29.01	36.04	12.5 m	0.56	1.80	4.81	12.59	31.85	40.61
24.3 m	0.34	0.97	2.34	5.52	12.64	15.70	21.6 m	0.22	0.72	1.91	5.00	12.64	16.12
28.0 m	0.28	0.79	1.89	4.46	10.21	12.68	24.9 m	0.17	0.56	1.50	3.93	9.95	12.68

The results indicated that for applying blasting methods ensuring a maximum allowable blasting vibration velocity of 12.7 cm/sec, as the charge weight per delay increased, a greater separation distance was required according to the test blasting results in comparison to the numerical analysis results (refer to Table 12 and Fig. 14).

3. Tunnel portal optimal design

3.1 Influencing factors

The tunnel portals are vulnerable to environmental damage due to the formation of large-scale cutting slopes and the application of retaining walls (K.E.C. 2002). In the construction process, excavation and blasting take place after reinforcing the slopes, which poses concerns for reduced stability due to proximity construction (K.E.C. 2009). Hence, designs must consider this, as continuous research has been conducted for improvements (Ahn *et al*. 2001, Moon and Shin 2008, Shin *et al*. 2009). However, specific details have not been provided.

Therefore, 3D numerical analysis of tunnel portals and case studies in design were utilized as foundational data for establishing optimal designs for tunnel portals (K.E.C. 2003, K.E.C. 2004). Through this process, factors influencing excavation, reinforcement, and stability design of the portals were classified as shown in Table 13.

3.2 Tunnel portal design considering influencing factors

The optimal design method for the tunnel portal, determined through numerical analysis and review of influencing factors, can be classified as follows:

• The height of the first bench on the back side of the tunnel portal is planned to be 15 meters or more.

• The installation of reinforced structures on the retaining wall is prohibited within 0.5 times the tunnel diameter (0.5D), as this section is where the plasticity area is generated due to tunnel excavation.

• When installing anchors on the back side of the tunnel portal, interference between the reinforced structures at the crown of the tunnel and the anchors is eliminated by adjusting the anchor installation angle.

Table 13 Influencing factors for the tunnel portal design

Category	Influencing factors
Reinforcement	Tunnel & slope reinforcement interference, reinforcement method (slope, tunnel)
Excavation	Blasting vibration, blasting noise, non-vibration excavation, etc.
Stability	Disturbed Zone, seismic stability, concrete lining structural stability
Rockfall / Landslide	History of landslide and debris flow, risk of rockfall
Slop of tunnel portal	The height of the first bench, the soil depth

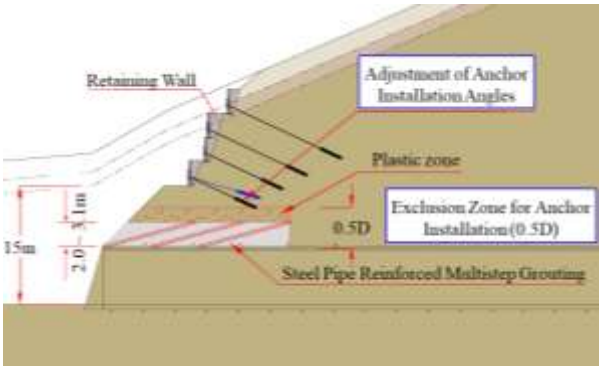

Fig. 15 Tunnel portal optimal design (conceptual)

Therefore, the arrangement and angle of the slope reinforcements (anchors, etc.) should be adjusted to ensure they are not installed within approximately 0.5D (D: tunnel diameter) of the tunnel crown. This consideration accounts for the plastic region and sections where excessive strain occurs during excavation.

4. Conclusions

In this study, research was conducted to minimize damage caused by blast vibrations in tunneling and cutting slopes where proximity blasting occurs, aiming to establish optimal design solutions. The following conclusions were drawn from this study:

• Despite the active application of slope reinforcement in the design phase due to recent policies avoiding large-scale cutting slopes, performance degradation occurs after

construction impacts (such as earthquakes or blasting). This leads to a reduction in service life and structural stability.

• The Top-down reinforcement method carries the potential for damage due to blast vibrations to pre-constructed structures during construction stages. However, the current blast design has limitations in incorporating such damages.

• Through numerical analysis, potential damages resulting from charge weight per delay and separation distances were predicted. These were then applied to slope stability, evaluating the damage caused by tunnel excavation and slope blasting. It is anticipated that this evaluation can contribute to future slope blast design criteria considering tunnel blasting effects.

• An optimal design methodology for the tunnel portal considering blasting effects has been proposed. The arrangement and angle of the slope reinforcements should be adjusted to ensure they are not installed within approximately 0.5D (D: tunnel diameter) of the tunnel crown.

References

Ahn, M.S., Ryu C.H., Park, J.N. and Kwun, J.A. (2001), "A study on the safe blast design to increase slope stability", *Explo. Blast.*, **19**(1), 85-92.

Choi, J.S., Lee, J.M. and Jo, M.S. (2006), "A calculation of blasting load using input identification method & evaluation of structure's vibration in numerical analysis", *J. Korean Soc. Rock Mech.*, **16**(3), 232-240.

Deng, D., Lia, L. and Zhao, L. (2019), "Stability analysis of slopes under groundwater seepage and application of charts for optimization of drainage design", *Geomech. Eng.*, **17**(2), 181-194. https://doi.org/10.12989/gae.2019.17.2.181.

DL E&C (1998), *Analysis of blasting impact zones and blasting design reports through test blasting*, DL E&C, Seoul, Republic of Korea.

Hu, G., Xia, Y., Zhong, L., Ruan, X. and Li, H. (2023), "Study on collapse mechanism and treatment measures of portal slope of a high-speed railway tunnel", *Geomech. Eng.*, **32**(1), 111-123. https://doi.org/10.12989/gae.2023.32.1.111.

Jin, Y., Kim, D., Jeong, S. and Park, K. (2022), "Prediction of dynamic behavior of full-scale slope based on the reduced scale 1 g shaking table test", *Geomech. Eng.*, **31**(4), 423-437. https://doi.org/10.12989/gae.2022.31.4.423.

K.E.C. (2002), *Review of design criteria for tunnel portal sections for environmentally friendly expressway construction*, Korea Expressway Corporation, Gimcheon-si, Gyeongsangbuk-do, Republic of Korea.

K.E.C. (2003), *Review of design criteria for tunnel portals*, Korea Expressway Corporation, Gimcheon-si, Gyeongsangbuk-do, Republic of Korea.

K.E.C. (2004), *Review and enhancement of design criteria for tunnel portals*, Korea Expressway Corporation, Gimcheon-si, Gyeongsangbuk-do, Republic of Korea.

K.E.C. (2009), *Review of vibration management criteria for reinforced soil retaining walls*, Korea Expressway Corporation, Gimcheon-si, Gyeongsangbuk-do, Republic of Korea.

K.E.C. (2019), *Review of proximity blasting criteria for retaining wall [00 Expressway]*, Korea Expressway Corporation, Gimcheon-si, Gyeongsangbuk-do, Republic of Korea.

K.E.C.R.I. (2017), *Approach for selecting optimal slopes for cutting slopes,* Korea Expressway Corporation Research Institute, Hwaseong-si, Gyeonggi-do, Republic of Korea.

Kim, D., Ko, J. and Kim, J. (2023), "Application of UAV images for rainfall-induced slope stability analysis in urban areas", *Geomech. Eng.*, **33**(2), 167-174. https://doi.org/10.12989/gae.2023.33.2.167.

Kim, N.Y. and Lee, K.H. (2021), *Damage evaluation of slope stabilization due to blasting*, Korea Expressway Corporation Research Institute, Hwaseong-si, Gyeonggi-do, Republic of Korea.

Lee, H., Kang, C.W. and Ko, J.S. (2011) "A study on prediction of ground vibration by near field blasting", *Explo. Blast.*, **29**(2), 32-42.

Min, H.D., Jeong, M.S., Song, Y.S. and Park, Y.S. (2005), "Blasting design methods considering the characteristics of blasting sites(Ⅱ)", *J. Korean Tunn. Undergr. Sp. Assoc.*, **7**(4), 63-80.

M.L.I.T. (2010), *Road design manual*, Ministry of Land, Infrastructure and Transport, Sejong City, Republic of Korea.

M.L.I.T. (2020), *The guideline for tunnel blasting design, construction, and management*, Ministry of Land, Infrastructure and Transport, Sejong City, Republic of Korea.

Moon, H.K. and Shin, J.H. (2008), "Effect of blast-induced vibration on a tunnel", *J. Korean Tunn. Undergr. Sp. Assoc.*, **10**(3), 207-219.

Shin, J.H., Moon, H.K., Choi, K.C. and Kim, T.K. (2009), "Evaluation of the blast-restriction zone to secure tunnel lining safety", *J. Korean Tunn. Undergr. Sp. Assoc.*, **11**(1), 85-95.

Starfield, A.M., Pugliese, J.M. (1968), "Compression waves generated in rock by cylindrical explosive charges: A comparison between a computer model and field measurements", *Int. J Rock Mech. Min. Sci.*, **5**(1), 65-77. https://doi.org/10.1016/0148-9062(68)90023-5.

Tran, A.T.P., Kim, A.R. and Cho, G.C. (2019), "Numerical modeling on the stability of slope with foundation during rainfall", *Geomech Eng.*, **17**(1), 109-118. https://doi.org/10.12989/gae.2019.17.1.109.